Chapter 8
All-Optical X-Ray and γ-Ray Sources from Ultraintense Laser-Matter Interactions

Leonida A. Gizzi

Abstract With the dramatic recent development of ultraintense lasers, a new perspective for compact, all-laser driven X-ray and γ-ray sources is emerging, aiming at a brightness currently achievable only with state of the art free electron lasers and Thomson scattering Sources based on large linear accelerators. In contrast with existing sources, all-optical sources exploit laser-plasma interaction to obtain the required high energy electrons to generate radiation. Bremsstrahlung or fluorescence emission driven from fast electron generation in laser interaction with solids was demonstrated to provide effective ultrashort X-ray emission with unique properties. More recently, laser-driven electron acceleration from interaction with gas-targets is being considered in place of conventional radio-frequency electron accelerators for a variety of radiation emission mechanisms. Broadband radiation generation schemes including betatron and Bremsstrahlung are being developed while free electron laser and Thomson scattering by collision with a synchronized laser pulse are being proposed for the generation of narrow band radiation. Here we present an overview of the current developments in this field.

8.1 Introduction

The impressive progress of high power laser technology initiated by the introduction of the Chirped Pulse Amplification (CPA) concept [1] is now leading to the realization of new large laser systems within the framework of the Extreme Light Infrastructure (ELI) that, by the end of this decade, will start paving the way to the exploration of new physical domains towards the electron-positron pair creation and the possibility to reach the critical field of quantum electrodynamics [2]. At the same time, the control of ultra-high gradient plasma acceleration [3–5] is being pursued and advanced schemes are being proposed for the future TeV linear collider [6].

L.A. Gizzi (✉)
Consiglio Nazionale delle Ricerche, Istituto Nazionale di Ottica, Pisa, Italy
e-mail: la.gizzi@ino.it

A. Giulietti (ed.), *Laser-Driven Particle Acceleration Towards Radiobiology and Medicine*, Biological and Medical Physics, Biomedical Engineering, DOI 10.1007/978-3-319-31563-8_8

Meanwhile, existing laser-plasma accelerating scheme are being considered for the development of novel radiation sources. All-optical X-ray free electron lasers (X-FEL) are already being explored [7] with encouraging chances of success in the medium term. In this context, a design for a new European Research Infrastructures of the H2020 Framework Programme named European Plasma Research Accelerator with eXcellence In Applications (EuPRAXIA) has recently being established. The programme [8] aims at developing compact and advanced X-ray sources based upon laser-plasma acceleration. Meanwhile, more affordable configurations, still based upon laser-driven high energy electrons, including Bremsstrahlung, Betatron and Thomson/Compton scattering are being explored, established and applied to different fields. Here we describe these techniques in which X-rays and γ-rays are produced using entirely optical techniques and based upon compact and scalable schemes, with a special attention to Thomson/Compton scattering. Before entering the discussion of radiation processes, an introduction to the basic ultraintense laser-plasma physics is given with attention to the conditions required for laser-plasma acceleration.

8.2 Basic Physical Processes

When an intense, short laser pulse is focused on matter, either a solid or a gas, a range of physical processes takes place which depend on the laser pulse parameters like peak intensity, overall pulse duration, wavelength, spot size, just to cite the most relevant. At the highest intensities available today, special consideration also needs to be given to the detailed temporal evolution of the laser pulse, including the so-called pre-pulses, the nanosecond-pedestal-to-short-pulse contrast and the picosecond-pedestal-to-short-pulse-contrast. Key applications of intense, short laser pulses are quite diverse and include Laser Plasma Acceleration (LPA) [9], ultrashort K-α X-ray sources [10], laser driven ion acceleration in the Target Normal Sheath Acceleration (TNSA) [11], and, going further up in intensity scale, the Fast Ignition (FI) approach [12, 13] to inertial confinement fusion (ICF). All these mechanisms have in common the ability of intense laser pulses to accelerate electrons with different basic mechanisms. A brief description of these mechanisms is given below.

8.2.1 Laser-Plasma Acceleration

In LPA a high intensity ultra-short pulse is focused in a gas to induce laser wakefield acceleration (LWFA) [9]. In the classical picture of LWFA, a longitudinal electron plasma wave is excited by the ponderomotive force associated to the laser pulse. The electron plasma wave exhibits a longitudinal electric field and has a

phase velocity set by the group velocity of the laser pulse, $v_g = c(1 - \omega_p^2/\omega_L^2)^{1/2}$, where $\omega_p = (n_e e^2/\varepsilon_o m_e)^{1/2}$ is the electron plasma frequency, with n_e being the electron plasma density, e, m_e and ε_o the electron charge and mass and the dielectric constant respectively and ω_L is the laser angular frequency. Electrons in phase with the wave are accelerated until, travelling faster than the electron plasma wave, overcome the accelerating field of the wave and start experiencing a decelerating field. This mechanism yields a maximum accelerating distance equal to the so-called dephasing length, given by:

$$L_d = \frac{\omega_L^2}{\omega_p^2}\lambda_p \simeq 3.2\, n_{18}^{-3/2}\, \lambda_{\mu m}^{-2}, \tag{8.1}$$

where n_{18} is the electron density in units of 10^{18} cm^{-3} and $\lambda_{\mu m}$ is the laser wavelength in micrometers. At high laser intensity, this classical scenario is significantly modified and numerical simulations provide detailed description of plasma wave excitation and evolution as well as electron injection and acceleration. The most compact configuration to obtain GeV-range electron bunches from laser-plasma interaction is based upon a gas-jet of a few millimeters, working in the so-called blowout regime [14, 15]. As shown in Fig. 8.1 (right), a short ($c\tau < \lambda_p/2$) and intense ($a_0 > 2$) laser pulse expels the plasma electrons outward creating a bare ion column. The blown-out electrons form a narrow sheath outside the bubble and the space charge generated by the charge separation pulls the electrons back creating a bubble-like wake whose size is $\lambda_b \simeq 2\sqrt{a_0}c/\omega_p$ and the dephasing length becomes $L_d = 2/3(\omega_L^2/\omega_p^2)\lambda_b$. Here $a_0 = eA_L/mc^2$ is the normalized vector potential of the laser. For sufficiently high laser intensities ($a_0 > 3.5 \div 4$) electrons at the back of the bubble can be injected in the cavity and experience a maximum

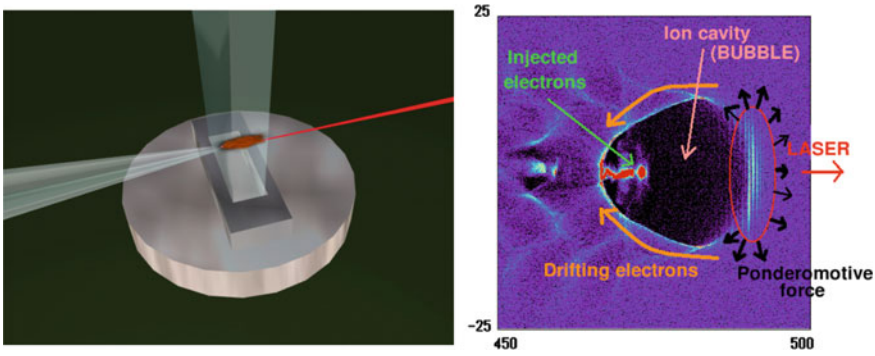

Fig. 8.1 Laser-gas interaction. *Left* Artist's view of laser interaction with a gas-jet. *Right* Plot of the electron density showing the cavity ion cavity generated by the intense laser propagating behind the laser pulse. The electron bunch injected in the bubble and accelerated by the longitudinal electric field is also visible

accelerating field of $E_{acc}[\mathrm{GW}] \simeq 100\, n_{18}^{1/2}$. Therefore, the maximum energy gain is given by [16]

$$W_{max}[\mathrm{GeV}] = E_{acc} L_d \simeq 0.37\, P_{TW}^{1/3}\, n_{18}^{-2/3}, \tag{8.2}$$

It can be shown that, according to this result, a matched condition (acceleration over the entire dephasing length) to achieve 1 GeV electron energy requires an electron density of 2×10^{18} cm^{-3}. At this relatively high electron density, experiments show that laser beam quality is the key parameter to enable a satisfactory propagation, but a range of processes still play a crucial role in the propagation. Diagnostic techniques aimed at characterizing the propagation dynamics and unveiling the microscopic features of accelerating structures in the plasma are therefore needed to gain control over the acceleration process. In this context, special attention is being dedicated to the control of self-injection of electrons. Recently, several mechanisms have been identified and implemented to control injection of electrons in a well-formed wake wave. These mechanisms can be broadly divided into three categories depending on the basic physical process responsible for injection as shown in Fig. 8.2. Here the objective is to achieve a localized injection of electrons with a limited longitudinal spatial extent, to ensure reduced energy spread of accelerated electrons. Wave-breaking is certainly the most fundamental process leading to injection of electrons in a plasma wave. While transverse wave breaking [17] suffers from a delocalized injection of electrons and consequently large energy spread, longitudinal wave breaking via down-ramp [18] density-transition [19] certainly provides more localized injection and limited energy spread of electrons. Activation of such injection schemes required accurate control on shape and profile of electron distribution that can be achieved using custom gas targets and plasma tailoring. Recent successful implementations of this principle yielding very localized injection have been demonstrated which rely on plasma lensing [20] and shock-front in gas-jets [21].

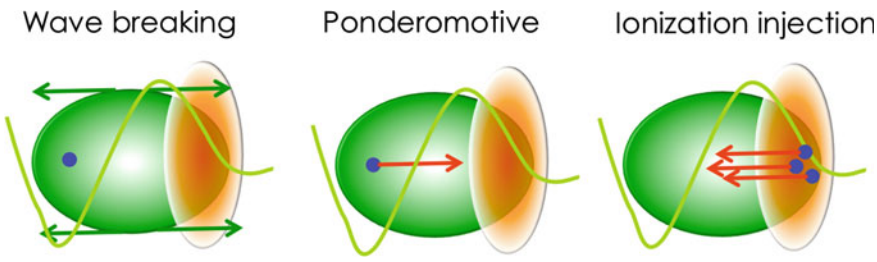

Fig. 8.2 Principal electron injection mechanisms divided schematically according to the underlying fundamental physical process currently being explored to provide localized injection and narrow electron energy spread

Ponderomotive injection [22, 23] also enables a high degree of control on the exact location of injection, but requires significantly more complex experimental configurations with additional laser pulses. In contrast, a simple technique to enhance electron injection is the so-called ionization-injection [24] in which field ionization properties of some gases are exploited to increase electron density in the bubble only at the peak of the pulse. Recent advances of this scheme also enable control of the spatial distribution of ionization injection and consequent smaller energy spread. Indeed, it is the dramatic development of these injection techniques which is currently enabling generation of narrow energy spread electrons with high energy, up to the multi GeV, uniquely by laser techniques. More effort is needed in this direction and perspectives in the near future are that injection and acceleration up to the 5 GeV energy range will be stable and accurate as required to drive a new generation of radiation sources for applications.

8.2.2 *Laser-Solid Interactions*

Interaction with a solid is fundamentally different from the interaction with a gas, mainly because the plasma produced by the interaction has a density greater than the critical density $n_c = m_e\omega_L^2/4\pi e^2 \simeq 1.1 \times 10^{21}\lambda_{\mu m}^{-2}\mathrm{cm}^{-3}$. Therefore, laser light cannot propagate in the solid and is reflected at the critical density layer. At high intensity, i.e. for $a_0 > 1$, relativistic effects start to play a role due to the relativistic mass increase of the electrons oscillating in the e.m. field. Consequently, the critical density increases and laser light can propagate at higher densities than the non-relativistic case, up to densities approximately equal to $n_{cr}^* \simeq (1 + a_o^2)^{1/2} n_{cr}$. However, for a_0 values accessible today, $n_{cr}^* \ll n_{solid}$, and laser light propagation in the bulk is limited to the skin depth, typically tens of nanometers. In these circumstances, energy can penetrate deep in the target via the so-called fast electrons. These fast electrons are heated/accelerated by the laser in the interaction region at the vacuum-solid interface due to a variety of mechanisms including laser-driven plasma instabilities, resonance absorption, vacuum heating, the so-called Brunel effect [25], the $\mathbf{J} \times \mathbf{B}$ heating [26] and so on.

Both the TNSA ion acceleration, X-ray K-α sources and the Fast Ignition scenario rely on fast electron generation and propagation in dense regions of the target. In these schemes there is a great interest in understanding how fast electrons are produced, how they propagate in the target substrate, how they transfer their energy to the dense/compressed material, what is the production efficiency and what fraction of their energy can be transferred to the target. All these processes depend strongly upon the conditions that the laser pulse finds initially on the target surface and once generation of the electrons begins, their transport will be affected by several mechanisms including the electron beam parameters and the resistivity of the material. In the case of very intense laser pulses, the energy distribution of these fast electrons is found to be Maxwellian, with a characteristic parameter T_h which

increases with the laser intensity. Ponderomotive force associated with the laser pulse is expected to give rise to an efficient generation of fast electrons. However, experiments of laser interaction with solid targets show scaling with the laser intensity like the so-called Beg's law [27]:

$$T_{hot}(\mathrm{MeV}) = 0.215\left[I_{18}\,\lambda_{\mu m}^2\right]^{1/3} \tag{8.3}$$

where I_{18} is the laser intensity in units of 10^{18} W/cm^2 and $\lambda_{\mu m}$ is the laser wavelength in μm. This law predicts a much weaker scaling than the ponderomotively driven fast electron temperature $T_{hot} \propto \left[(1+cI)^{1/2}-1\right]$ found in Particle-in-Cell simulations [28]. The lower scaling suggests that other mechanisms including resonance absorption could be playing a role, but a full understanding of this process is still lacking. A theoretical model has been developed [29] which shows a good agreement with Beg's law and predicts very high laser absorption at high intensities. More recently [30] a model was developed in which energy of fast electrons is found to increase with the scalelength of a preformed plasma in front of the solid target, suggesting that the counter-propagating incident and reflected light in the plasma should be taken into account. The role of counter-propagating incident and reflected light is also invoked in another recent modelling of interaction with steep density gradients [31].

Incidentally, it is worthwhile observing that fast electrons are expected to play an important role in the ICF fast ignition scheme [12] and experimental and theoretical effort world wide is aimed at studying the dynamics of fast electron generation and propagation in solids and plasmas. Scaled experiments are currently possible [32] which provide a preliminary assessment of the role of a fast ignition pulse in moderately compressed spherical pellet. At the same time several experiments use even simpler configurations in which the attention is focused on some specific processes involved in the fast ignition concept. In these experiments, laser pulses are focused to reach the highest possible intensity, typically close to 10^{20} W/cm^2. At these intensities, a great role is played in the interaction process by the specific properties of the laser pulse including the beam quality and temporal contrast and knowledge of these features is therefore needed to model the experimental results with presently available numerical codes.

On the other hand, energetic electrons are responsible for emission of X-ray radiation characteristic of the atomic constituents of the target. In fact, while penetrating into the underlying cold target material, they knock out electrons preferentially from the inner electronic shells of the atoms or ions [33]. The radiative transitions of electrons from the outer shells finally leads to the generation of characteristic K-lines. The role of different mechanisms responsible for the generation of fast electrons is clearly visible from polarization dependent studies [34] which show strong reduction of emission for linearly S-polarized and circularly polarized radiation compared to linearly P-polarized radiation (Fig. 8.3).

This is just an example of the interplay between laser radiation properties and K-α emission which makes this type of radiation from laser-solid interaction of a

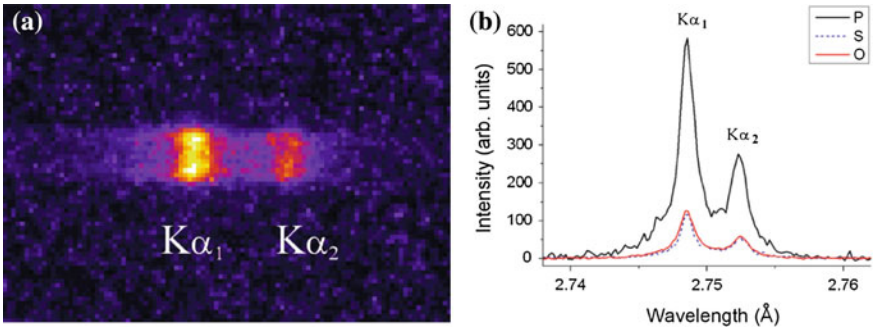

Fig. 8.3 **a** Raw spectrum of fluorescence Ti K-α emission from laser irradiation of a Ti foil at moderately relativistic intensity ($a_o \simeq 1$), obtained by averaging 100 p-polarized laser pulses. **b** Ti K-α spectra obtained by different laser pulse polarizations, and obtained by averaging 100 laser shots (after [34])

great interest. In general, K-α emission spectroscopy of neutral or partially ionized atoms, possibly with spatial resolution, can be exploited for studying the fast electron transport through matter with micrometer resolution [35]. Consequently, from the point of view of applications as a radiation source, the main characteristics of K-α based ultrashort X-ray emission, such as photon yields as well as duration and size, strongly depend upon the production and transport processes of the fast electrons. The understanding of these issue plays a crucial role in laser-plasma based K-α sources and their applications and is the subject of current investigations using advanced numerical and experimental tools.

In recent years, effort in this context is directed towards the enhancement of laser-plasma coupling using micro and nano-engineered target which, in many cases, have been found to exhibit larger absorptivity of laser radiation (see [36] and references therein) or resonant excitation of surface plasma waves [37]. The specific properties of nano-structures required to influence fast electron generation are still being explored and a general understanding of governing parameters and scaling laws is still lacking. However, important milestones have been established concerning the fundamental role of laser contrast in enabling absorption and heating of dense plasma [38] by nano-structured targets. These recent observations are triggering the development of an entirely new class of radiation sources which promise to extend significantly the realm of X-ray emission from femtosecond laser solid interactions, with the possibility of activating a micro plasma waveguide capable of efficiently accelerating electrons and acting like wigglers to generate bright hard X-ray emission [39]. Although numerical and experimental investigations in this context of micro and nano plasmonics are still in their infancy, current trends promise major impact of these studies on future compact X-ray and γ-ray sources for applications.

8.3 Bremsstrahlung from Laser-Driven Electrons

If a charged particle makes a Coulomb collision with the nucleus of an atom, it undergoes acceleration and emits radiation with a continuous photon energy spectrum that extends up to approximately the electron rest energy times the γ factor of the incident electron. For value of $\gamma > 1$, the photons are emitted in the forward direction in a cone of aperture of approximately $1/\gamma$. The total radiated power scales as Z^2 and can account for a conversion of a significant fraction of the electron energy into photon energy. Practical Bremsstrahlung sources extend from the keV range, as in the X-ray tube, up to the multi MeV range. In the latter case, the high energy electron bunch, accelerated by a linac, hits a converter, typically a tungsten or a tantalum plate, and generates γ-rays with photon density as high as 1 ph/eV/sec. Alternatively, high energy electron bunches produced using compact plasma accelerators driven by lasers can be used in place of linac generated electrons. All-optical, laser-based bremsstrahlung X-ray and γ-ray sources have already been explored [40, 41] and successfully tested using self-injection electron bunches [42, 43]. Figure 8.4 shows a schematic set up of a typical laser-driven γ-ray source used in [43]. Here the source was used to activate a gold sample in the 8–17.5 MeV photon energy range of the giant dipole resonance. A total flux of 4×10^8 photons per Joule of laser energy was estimated through activation measurements which makes this class of sources the brightest Bremsstrahlung source in the considered photon energy range [44].

In this context, photon yield can be significantly enhanced if multiple bunches are generated in laser wakefield acceleration for a single laser pulse. In fact, in the experimental conditions explored in [44], the laser pulse undergoes self-phase modulation and compression that leads to the excitation of a non-linear plasma wave with multiple buckets with a similar amplitude. Injection and acceleration occurs in each bucket and consequently, multiple electron bunches of high energy electrons are generated at each laser shot as shown in Fig. 8.5.

A similar set up is being considered for other applications like imaging and non destructive testing of thick objects. In this case the source size is a very relevant parameter that must be optimized to enhance spatial resolution of the imaging technique. Recent studies [45] show that a source size as small as 30 μm can be obtained placing the Bremsstrahlung converter a few millimetres from the gas-jet downstream

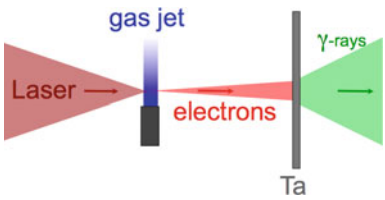

Fig. 8.4 A schematic set up of a Bremsstrahlung source based upon a laser-plasma source of high energy electrons. A Tantalum converter is placed in the proximity of the gas-jet target where the transverse size of the laser accelerated electron bunch is as small as a fraction of a millimetre

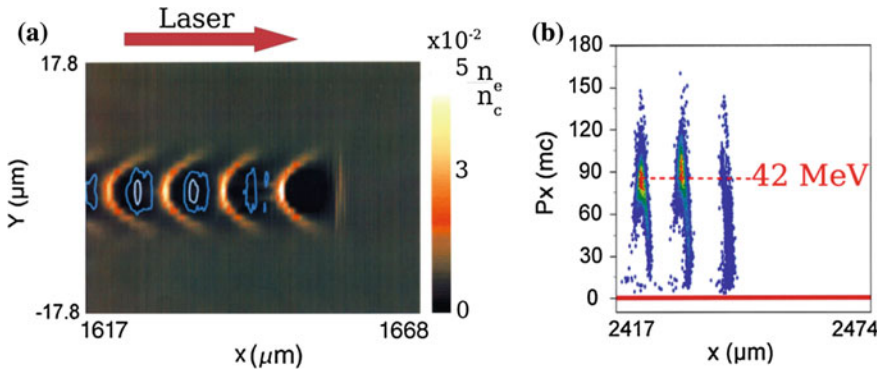

Fig. 8.5 Particle-in-cell simulation of non-linear wakefield excitation and acceleration of multiple bunches. This regime, explored in [44] provides efficient conversion of laser energy into high energy electrons and Bremsstrahlung radiation

the bunch propagation direction to perform high resolution γ-ray imaging of bulky and dense objets [46]. An additional feature of all-laser driven sources is the intrinsic ultrashort pulse duration which, combined with the potentially high degree of compactness, makes this class of sources unique and potentially advantageous for applications in a wide range of fields, both in industry and in basic research.

8.4 Betatron in Laser-Wakefield Acceleration

Another very effective mechanism of generation of X-ray radiation during laser-plasma wakefield acceleration originates from the transverse oscillation of the electron bunch in the acceleration cavity due to the strong restoring force directed towards the longitudinal laser propagation axis as shown schematically in Fig. 8.6. The typical photon energy of this emission is similar to the undulator type radiation characterised by a wavelength of the oscillation $\lambda_\beta = \sqrt{2\gamma_0}\,\lambda_p$, where $\lambda_p = 2\pi c/\omega_p = 3.34 \times 10^{10} n_e^{-1/2}$ μm is the electron plasma wavelength, with n_e being the electron plasma density in units of cm^{-3}. Photon energy up to the keV range can be easily achieved for electron energy up to 1 GeV.

This radiation mechanism was first observed in 2004 [47] and is currently being regarded as a very promising source for X-ray imaging up to the keV range. In fact, the effective small source size typical of this emission process makes phase contrast image possible as recently demonstrated both at 5 keV [48] and earlier at higher photon energies of 10 keV [49] and above 20 keV approximately [50]. Although betatron emission typically exhibits a broadband spectrum in the keV range, higher photon energy can be achieved in conditions of enhanced transverse electron oscillations as demonstrated in [51] where parameters of the accelerating cavity were modified in such a way to enable overlapping of the electrons with the rear of the laser pulse. In this way the betatron motion was resonantly excited and

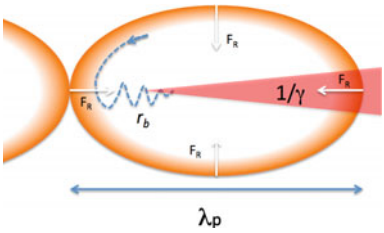

Fig. 8.6 A pictorial view of the physical principle behind the betatron radiation emission. Electrons injected in the longitudinal field of the accelerating bubble-like structure oscillate around the axis due to the restoring force and emit radiation in the forward direction

the resulting oscillation amplitude was found to increase significantly, leading to an enhanced X-ray photon energy.

8.5 Thomson Scattering

Ideally, nuclear applications require high energy and spectral density γ-rays. In this scenario, a very demanding application is the Nuclear Resonance Fluorescence (NRF) due to the small spectral width of nuclear resonance transitions (Fig. 8.7).

Once excited, the nucleus will emit characteristic fluorescence γ-rays which will depend upon the specific atomic element and isotopes [53] is. This is the principle behind the use of such a technique for safety and inspection applications. The ideal requirements for NRF applications on the gamma ray beam are bandwidths as small as possible (desired <0.1 %, present state of the art 2 %) and spectral density as high as 10^4 ph/sec/eV. These requirements are very challenging and new large installations based on state-of-the-art accelerator technology are being proposed to fulfill them. The estimated cost of such installations is currently in the 50–100 Meuro. Such new sources [54] are based upon the use of high energy Linacs and high power lasers or free electron lasers [55] to generate γ-rays via Thomson/Compton scattering. In this scenario, the use of laser-plasma accelerated electrons has also been explored [52] and is regarded as a possible way to make radiation sources far more accessible than current Linac based sources.

All-optical Thomson scattering is being considered in which a high intensity laser pulse is set to collide with a laser-accelerated electron bunch. In a pioneering experiment [56] carried out at the Jena laser Facility in 2006, all-optical Thomson scattering (TS) in the 1 keV X-ray region was first demonstrated using a compact configuration with a limited freedom for optimization and using poor quality laser-accelerated electron bunches, still affected by 100 % energy spread. Since then, laser-plasma acceleration has seen a dramatic improvement and laser accelerated electrons can now exceed 4 GeV peak energy [57] with energy spread well below 10 %, with record values close to 1 %. Moreover, new schemes are being proposed to control injection and optimize acceleration, which are now being

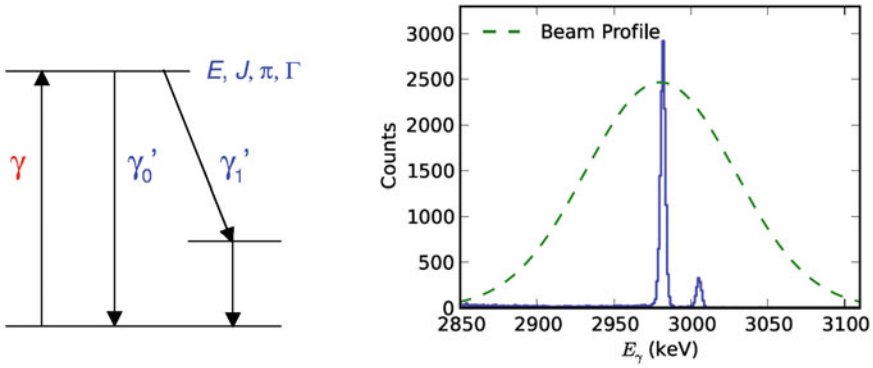

Fig. 8.7 Nuclear resonance fluorescence is based upon the detection of characteristic fluorescence emission (*right*) with a high intensity γ-ray beam, resulting from decay of nuclei after *γ*-ray excitation (*left*). It is used to identify isotopes and can be applied to safety and inspection. Typical excited states of nuclei lie in the MeV range and have linewidths of <1 eV (after [52and 53 is])

implemented to further improve the quality of laser accelerated electrons. These improvements are rapidly reflecting in the development of all-optical Thomson scatterig sources as described below.

Thomson scattering from free electrons is a pure electrodynamics process in which each electron radiates while accelerating under the action of an external electromagnetic wave. If the electron is at rest or is not relativistic, the magnetic field of the e.m. wave can be neglected and the motion is entirely due to the electric field. The electron oscillates along the electric field direction and emits e.m. dipole radiation. For an electron with a velocity $\beta \ll 1$ and acceleration $\dot{\beta}$, the power of the radiation emitted per unit solid angle is given by the following expression [58]:

$$\frac{dP}{d\Omega} = \frac{e^2}{4\pi c}|\mathbf{n} \times (\mathbf{n} \times \dot{\beta})|^2 \tag{8.4}$$

which, via integration over the entire solid angle, yields the well known Larmor formula of the total radiated power for a non relativistic accelerated electron:

$$P = \frac{2}{3}\frac{e^2}{c^3}|\dot{\mathbf{v}}|^2. \tag{8.5}$$

Radiation is emitted in directions other than that of the linearly polarized incident plane wave and the radiation frequency is the same as the incident radiation. In terms of the radiation intensity I, and the density of scattering electrons n_e, the emission coefficient is given by:

$$\varepsilon = \frac{\pi\sigma_T}{2} I n_e \tag{8.6}$$

where σ_T is the so-called Thomson cross section:

$$\sigma_T = \frac{8\pi}{3}\left(\frac{e^2}{m_e c^2}\right)^2 = 6.65 \times 10^{-25}\,\mathrm{cm}^2 \tag{8.7}$$

with the quantity $r_e = e^2/m_e c^2$ being the classical electron radius. This is the situation typically used to detect propagation of laser pulse in an under dense plasma like in [59] or to measure the plasma properties [60].

If the scattering electron is moving at a relativistic velocity, the energy radiated per unit solid angle per unit frequency interval is instead given by [58]:

$$\frac{dI^2}{d\Omega d\omega} = \frac{e^2}{4\pi^2 c}\left|\int_{-\infty}^{+\infty} \frac{\mathbf{n}\times[(\mathbf{n}-\beta)\times\dot{\beta}]}{(1-\beta\cdot\mathbf{n})^2}\, \mathrm{e}^{i\omega(t-\mathbf{n}\cdot\mathbf{r}(t)/c)} dt\right|^2 \tag{8.8}$$

which, compared with the non-relativistic case of (8.4), increases indefinitely when $\beta\cdot\mathbf{n} \to 1$ which occurs when $\beta \simeq 1$ and β is parallel to $\mathbf{n}$. In this case, the scattering e.m. radiation in the particle rest frame will be Doppler shifted by a factor γ. Also, radiation emitted by the electron will be Doppler shifted in the laboratory frame resulting in a total upshift of a factor γ^2. Also, the Lorentz transformation from the particle rest frame to the laboratory frame implies that the radiation will be emitted along the direction of the electron velocity in a small cone of aperture $\Delta\theta \simeq 1/\gamma$ around the velocity vector direction.

8.5.1 Scattering Parameters

We consider the geometry described in Fig. 8.8. The three main parameters governing the scattering process are the electron energy $E_o = \gamma_o m_e c^2$, the laser pulse

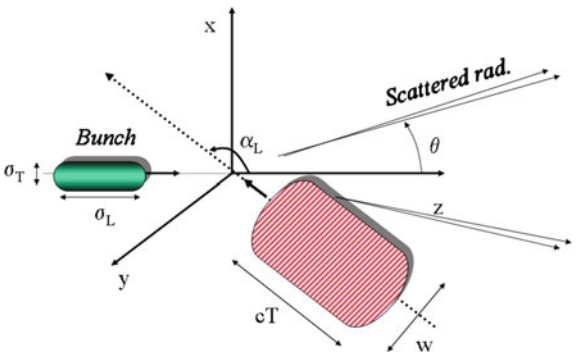

Fig. 8.8 Thomson scattering geometry. The scattered radiation is emitted along the z axis, in a small cone of aperture $1/\gamma$. When $\alpha_L = \pi$ the backscattering geometry occurs

peak normalized amplitude $a_o = eA/(m_e c^2) \approx 8.5 \times 10^{-10}\sqrt{I\lambda_{\mu m}^2}$, I being the laser peak intensity in W/cm^2, $\lambda_{\mu m}$ is the laser wavelength in μm and α_L is the angle between the propagation directions of the laser pulse and the electrons.

The pulse amplitude controls the momentum transferred from the laser pulse to the electron, i.e. the number of photons of the pulse absorbed by the electron.

8.5.1.1 Linear Regime

If $a_o \ll 1$, only one photon is absorbed and the resulting electron motion always admits a reference frame in which the quivering is non-relativistic (linear Thomson scattering) [61]. Assuming $\gamma_o \gg 1$, scattered radiation is emitted forward with respect to the electron initial motion within a cone of aperture $1/\gamma_o$. Assuming a laser pulse having a rise time much greater than the pulse period, the resulting scattered radiation ω_γ is spectrally shifted compared to the laser frequency ω_L at a peak energy given by [62]:

$$\omega_\gamma \cong 2\gamma_o^2(1 - \cos\alpha_L)\omega_L \tag{8.9}$$

Among the possible interaction geometries, the case of backscattering $\alpha_L = \pi$ is the most suitable for at least three aspects: (i) it produces photons with the highest energy

$$\omega_\gamma \cong 4\gamma_o^2\omega_L; \tag{8.10}$$

(ii) it allows the highest overlap of the electron beam and the pulse; (iii) it minimizes spurious effects induced by the transverse ponderomotive forces of the laser pulse.

The number of scattered photons and the spectral distribution of the radiation collected within a cone of aperture θ depend on the pulse parameters, the bunch quality and the product. A simplified formula, which is valid in the case of negligible beam emittance and linear scattering can be found in [61] and reads:

$$N_{TS,Linear} = \frac{1}{2}FN_e\alpha\omega_L T a_o^2\psi^2\frac{1+\psi^2+2/3\psi^4}{(1+\psi^2)^3} \tag{8.11}$$

where N_e is the number of electrons in the bunch, F the filling factor which depends on both the pulse and electron bunch envelopes, T is the laser pulse duration, ψ is the collection aperture angle, and $\alpha = 1/137$ the fine structure constant. Note that when $\psi \ll 1$, then $N_{Sc} \propto \psi^2$ indicating the strong dependence of the collected photons upon the collection aperture.

If we collect over the entire solid angle $\theta_{max} = 1/\gamma_o$, the formula of (8.11) simplifies to:

$$N_{TS,Linear} \cong 1.2 \times 10^{-3} F N_e \omega_L T a_o^2 \tag{8.12}$$

which clearly shows the dependence of the total scattered photons upon the main experimental parameters. Assuming a filling factor $F = 1$, a number of electrons corresponding to a total charge of 100 pC, i.e. $N_e = 6 \times 10^8$ and a laser pulse duration of $T = 100$ fs, we find:

$$N_{TS,Linear} = 1.68 \times 10^7 a_o^2. \tag{8.13}$$

According to this formula we immediately find that, for a fixed pulse duration, the scaling of $N_{TS,Linear} \propto a_o^2$ requires a relatively high intensity. The detailed description of Thomson scattering of realistic electron bunches and laser pulses, in the linear or nonlinear regime, is now made possible by using Monte Carlo codes based on the analytic description of the single particle dynamics. Some results will be shown in the description of the proposed experiment given below.

8.5.1.2 Non-linear Regime

In the nonlinear regime, $a_0 \approx 1$, the resulting strong exchange between the laser pulse and electron momentum induces a complex and relativistic electron motion, consisting of a drift and a quivering having both longitudinal and transverse components with respect to the pulse propagation. In turn, the time dependent longitudinal drifting results in a non-harmonic electron motion that produces scattered radiation with a complex spectral distribution characterised by harmonics of the fundamental frequency. If the electron interacts with a laser pulse with a constant amplitude, e.g. a flat-top laser pulse, the spectral distribution of the scattered radiation consists of equally spaced harmonics [61]. In the case of head-on collision, the peak energy of each Nth harmonics in a back-scattering configuration reads now:

$$\omega_{\gamma,N} \cong N_{th} \frac{4\gamma_o^2 \omega_L}{1 + a_o^2/2}. \tag{8.14}$$

As the intensity increases even further ($a_0 \gg 1$), radiation is emitted into many closely spaced harmonics showing a typical synchrotron radiation spectrum. When considering scattering from an electron bunch, harmonics produced by each electron will be slightly shifted due to non-ideal beam effects like energy spread and beam emittance. As a consequence, a continuous spectrum is generated which extends up to the critical frequency that scales [63] as a_o^3.

8.5.1.3 Radiation Reaction Regime

In the classical description of Thomson scattering, the loss of energy and momentum of the particle carried away by the emitted radiation is neglected and the particle trajectory is calculated considering the external force $\mathbf{F}_{ext} = q(\mathbf{E} + v \times \mathbf{B}/c)$, where q is the charge of the particle. When the laser intensity increases further, the energy and the momentum lost by the particle emitting radiation increases up to the point where the effect on the particle trajectory cannot be neglected and must be included in the calculation. Simple considerations [58] show that in the case of electrons, this so-called radiation reaction regime requires that a significant loss of energy and momentum occurs on a time scale of the order of $\tau_{RR} \approx 10^{-24}$ s and a spatial scale of the order of $l_{RR} \approx c\tau \approx r_e$. These conditions are quite extreme and in typical laboratory experiments radiation reaction effects can be neglected. However, with current development, ultraintense lasers may soon be able to enter this regime. It can be shown that the above conditions are satisfied for a laser intensity $a_o > 400$ when the equation of motion of the electron must include an additional force to describe the radiation reaction is a self consistent way [64]. A physically satisfactory description of radiation reaction is given by the Landau-Lifshitz equation [65]. Experimental validation of this theory is still lacking and the experimental configuration used for all-optical Thomson scattering is regarded as an ideal test bed to evaluate the accuracy of the theory, even at values of the laser intensity below the above threshold [66].

8.5.2 Thomson Scattering in the Laboratory

Generation of radiation via Thomson scattering of a laser pulse by energetic counter-propagating electrons was initially proposed in 1963 [67, 68] as a quasi monochromatic and polarized photons source. With the development of ultraintense lasers the interest on this process has grown and the process is now being exploited as a bright source of energetic photons from UV to γ-rays and atto-second sources in the full nonlinear regime. Thomson scattering in the linear regime has also been proposed to attain the angular distribution of a monochromatic electron bunch [69]. Moreover, experimental methods have been proposed to measure the length of a monochromatic electron bunch and to measure the energy spectrum of a single bunch eventually characterized by a wide energy spread or alternatively to measure the angular distribution of a single bunch with a known energy spectrum [70]. These new experimental methods are based on X-ray detectors having both a good spectral and angular resolution (cooled CCD camera used in the single photon counting regime) [71].

In the typical all-optical configuration, two laser pulses are synchronized and then focused in a counter-propagating geometry. One of the pulses propagates towards the electron bunch generated by the other pulse, producing radiation propagating along the bunch propagation direction. The counter-propagating configuration is obtained either using two separately compressed laser pulses with

controlled energy or by splitting the main laser pulse in two pulses, with independent focusing configuration. In this case particular care must be taken in arranging the splitting configuration where one, or both laser pulses may suffer from phase front distortions introduced by the beam splitter.

According to (8.11), photon yield in the linear regime scales as a_o^2. Therefore, for a given transverse size of the electron bunch and FWHM of the laser pulse, we obtain the laser energy required in the scattering pulse to obtain optimum photon production. If we set $a_o = 0.3$, corresponding to an intensity of 2×10^{17} W/cm^2, we find that for realistic values of the scattering pulse focal spot diameter of 25 or 50 μm the energy required is 115 and 45 mJ respectively. This value increases up to almost 2 J for a FWHM of 100 μm. From the point of view of the accelerating laser pulse a stable self-injection with moderate energy spread requires $a_o > 1$ over a long distance in the plasma. This can be achieved with long focal length optics characterized by large diameter focal spots. Ultimately, a pulse energy exceeding 1 J for a 30 fs pulse duration is required. Both these conditions on the scattering and accelerating laser pulses suggest that the ideal laser system for the investigation of all-optical Thomson scattering is capable of delivering in excess of 2 J of energy, possibly in two independently controllable pulses.

Thomson scattering experiments require spatial and temporal overlap of the electron bunch and the scattering laser pulse at the collision point. In the case of laser-wakefield acceleration, location of the collision point relative to the acceleration region requires a careful evaluation based on the electron bunch cross section and scattering pulse focal spot and Raileigh length Z_R as shown in Fig. 8.9. Ideally, a collision point set just at the end of the accelerating region would avoid deterioration of electron bunch properties, In fact, free propagation of the accelerated bunch may result in an increase of transverse and longitudinal size, emittance and energy spread. However, at the exit of the accelerating region, electron bunches have very small transverse and longitudinal size, typically a few μm and a few fs which would set demanding conditions on the scattering laser pulse.

Current experiments typically use a collision point set a few mm downstream the accelerating region, where electron bunch transverse size is a few tens of μm, easily achievable with the scattering pulse. In the original paper by Chen et al. [72], the collision point was set 1 mm after the exit of the plasma, where the focal spot of the 800 nm scattering pulse spot size was 9 μm and the overlapping (emitting) region

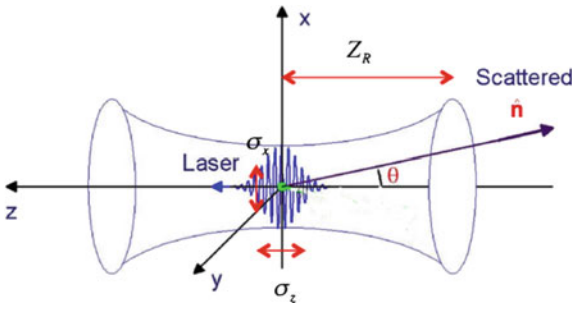

Fig. 8.9 Temporal and spatial overlapping of Thomson scattering pulse and electron bunch must be controlled to optimize X-ray scattering, taking into account electron bunch evolution beyond the accelerating region and scattering pulse focal spot and Raileigh length

was estimated to be 5 μm. Scattering with a 250 MeV cut-off energy electrons enabled generation of peak photon energy of 1.2 MeV. Sarri et al. [44] used a F/2 OAP to focus the 18 J, 42 fs scattering pulse 10 mm downstream of the exit of the gas target were the electron bunch transverse size was 30 μm and the average normalized intensity was $a_o = 2$. Scattering off LWFA electrons with energy up to 600 MeV resulted in Thomson scattering photons with energy up to 18 MeV, the highest energy obtained so far with all-optical Thomson scattering.

Liu et al. [73] achieved similar photon energy with lower peak electron energy, but using frequency doubled, 400 nm optical scattering pulse. They used a separate optical compressor to control focal spot quality of the frequency doubled pulse which is more sensitive to phase front distortions. They tuned the frequency doubled scattering pulse to produce 54 mJ in a 300 fs laser pulse, focused in a 15 μm focal spot and were able to achieve >9 MeV photon energy with a broadband spectrum peaked at approximately 400 MeV.

On the other hand, depending on the perspective application, tuneability of the X-ray photon energy may be an important option of a source. According to (8.10) or (8.14), the frequency of the scattered radiation can be tuned by changing either the electron energy or the scattering photon energy. Powers et al. [74] achieved tuneability changing the electron energy in the range from 50 to 200 MeV by changing the plasma density to exploit the square root dependence of the accelerating electric field upon the electron density that occurs in LWFA. In this way they were able to achieve tuneability in the range from 70 keV to approximately 1 MeV. Tunability in the 5–42 keV was demonstrated by Khrennikov et al. [75] using a different technique to tune electron energy. They use shock-front injection [21] which exploits the properties of sharp downramps of the electron density of the plasma [70] to localize electron injection. Tunability is achieved by shifting the position of the downramp along the plasma to control acceleration length.

Finally, special attention deserves the detection of X-ray and γ-ray radiation generated by all-optical Thomson sources. Current experiments show that peak brilliance of these sources in the MeV region exceeds 10^{20} photons s^{-1} mm^{-2} $mrad^{-2}$ 0.1 % bandwidth. Also, as discussed above, the spectral properties of these sources is of a great interest for investigation of scattering processes at high fields. Therefore, besides calorimetric measurements aimed at measuring the total scattered energy, detectors should enable accurate spectroscopic investigation. This can be achieved using the scintillation detectors in the single photon counting regime accumulating photons over many laser shots and assuming reproducibility of the source. In general, single shot measurements are required and current detection techniques are limited. One possibility [76] is to exploit the Compton scattering effect in low Z materials to convert γ-ray photons into electrons and recover the photon spectrum from the electron spectrum. Further development of these techniques will be required to enable accurate characterization of all-optical Thomson scattering sources.

In conclusion, we have given an overview of all-laser driven techniques for generation of X-ray and γ-rays, with a detailed discussion of Thomson scattering. In the multi MeV range, state of the art technology indeed exploit this mechanism to generate bright sources based upon large conventional accelerators. The dramatic

development of laser-based electron acceleration techniques is rapidly driving the practical demonstration of a new class of all-optical, compact radiation sources. Recent experiments clearly show increasing control over source properties and promise major achievements in the near future.

References

1. D. Stickland, G. Mourou, Opt. Commun. **56**, 219 (1985)
2. J. Schwinger, Phys. Rev. **82**, 664 (1951)
3. J. Faure, Y. Glinec, A. Pukhov et al., Lett. Nat. **431**, 541 (2004)
4. W.P. Leemans et al., Nat. Phys. **2**, 696 (2006)
5. D. Giulietti et al., Phys. Plasmas **9**, 3655 (2002). (letter)
6. W.P. Leemans et al., AIP Conf. Proc. **1299**, 3 (2010)
7. J.G. Gallacher et al., Phys. Plasmas **16**, 093102 (2009)
8. http://www.eupraxia-project.eu/home.html
9. T. Tajima, J.M. Dawson, Phys. Rev. Lett. **43**, 267 (1979)
10. A. Rousse et al., Phys. Rev. E. Stat. Phys. Plasmas. Fluids. Relat. Interdiscip. Top. **50**, 2200 (1994)
11. R.A. Snavely et al., Phys. Rev. Lett. **85**, 2945 (2000)
12. M. Tabak et al., Phys. Plasmas **1**, 1626 (1994)
13. S. Atzeni, J.M. ter Vehn, *The Physics of Inertial Fusion* (Oxford University Press, Great Clarendon Street, Oxford ***OX2 6DP, 2004)
14. A. Pukhov, J. ter Vehn, Appl. Phys. B **74**, 355 (2002)
15. S. Gordienko, A. Pukhov, Phys. Plasmas **12**, 043109 (2005)
16. B.B. Pollock et al., Phys. Rev. Lett. **107**, 045001 (2011)
17. S.V. Bulanov, F. Pegoraro, A.M. Pukhov, A.S. Sakharov, Phys. Rev. Lett. **78**, 4205 (1997)
18. S. Bulanov, N. Naumova, F. Pegoraro, J. Sakai, Phys. Rev. E **58**, 5257 (1995)
19. P. Tomassini et al., Phys. Rev. ST Accel. Beams **6**, 121301 (2003)
20. A.J. Gonsalves et al., Nat. Phys. **7**, 862 (2011)
21. A. Buck et al., Phys. Rev. Lett. **110**, 185006 (2013)
22. D. Umstadter, J.K. Kim, E. Dodd, Phys. Rev. Lett. **76**, 2073 (1996)
23. E. Esarey et al., Phys. Rev. Lett. **79**, 2682 (1997)
24. M. Chen, Z.-M. Sheng, Y.-Y. Ma, J. Zhang, J. Appl. Phys. **99** (2006)
25. S.C. Wilks, W.L. Kruer, M. Tabak, A.B. Langdon, Phys. Rev. Lett. **69**, 1383 (1992)
26. W.L. Kruer, K. Estabrook, Phys. Fluids **28**, 430 (1985)
27. F.N. Beg et al., Phys. Plasmas **4**, 447 (1997)
28. S.C. Wilks, W.L. Kruer, M. Tabak, A.B. Langdon, Phys. Rev. Lett. **69**, 1383 (1992)
29. M.G. Haines, M.S. Wei, F.N. Beg, R.B. Stephens, Phys. Rev. Lett. **102**, 045008 (2009)
30. B.S. Paradkar et al., Phys. Rev. E **83**, 046401 (2011)
31. J. May et al., Phys. Rev. E **84**, 025401 (2011)
32. W. Theobald et al., Phys. Plasmas **18**, 056305 (2011)
33. F. Ewald, H. Schwoerer, R. Sauerbrey, Europhys. Lett. **60**, 710 (2002)
34. G. Cristoforetti et al., Phys. Rev. E **87**, 023103 (2013)
35. L.A. Gizzi et al., Plasma Phys. Control. Fusion **49**, B221 (2007)
36. G. Cristoforetti et al., Plasma Phys. Control. Fusion **56**, 095001 (2014)
37. T. Ceccotti et al., Phys. Rev. Lett. **111**, 185001 (2013)
38. M.A. Purvis et al., Nat. Photonics **7**, 796 (2013)
39. L. Yi, A. Pukhov, P.L. Thanh, B. Shen **1**, 1 (2015)
40. L.A. Gizzi et al., Phys. Rev. Lett. **76**, 2278 (1996)
41. L.A. Gizzi et al., Laser Part. Beams **19**, 181 (2001)

42. D. Giulietti et al., Phys. Rev. E **64**, 015402(R) (2001)
43. A. Giulietti et al., Phys. Rev. Lett. **101**, 105002 (2008)
44. G. Sarri et al., Phys. Rev. Lett. **113**, 224801 (2014)
45. A. Ben-Ismal, J. Faure, V. Malka, Nucl. Instrum. Methods Phys. Res. Sect. A. Accel. Spectrom. Detect. Assoc. Equip. **629**, 382 (2011)
46. A. Ben-Ismal et al., Appl. Phys. Lett. **98**, 264101 (2011)
47. S. Corde et al., Rev. Mod. Phys. **85**, 1 (2013)
48. J. Wenz et al., Nat. Commun. **6**, 7568 (2015)
49. S. Kneip et al., Appl. Phys. Lett. **99**, 093701 (2011)
50. Z. Najmudin et al., Philos. Trans. A. Math. Phys. Eng. Sci. **372**, 20130032 (2014)
51. S. Cipiccia et al., Nat. Phys. **7**, 867 (2011)
52. W. Walsh et al., in *Nuclear Science Symposium Conference Record (NSS/MIC), 2009 IEEE* (IEEE, Orlando, FL, 2009), pp. 80–85
53. C.T.Angell et al., Phys. Rev. C 90, 054315 (2014)
54. F. Albert et al., Phys. Rev. ST Accel. Beams **13**, 070704 (2010)
55. A.M. Sandorfi et al., IEEE Trans. Nucl. Sci. **30**, 3083 (1983)
56. H. Schwoerer et al., Phys. Rev. Lett. **96**, 014802 (2006)
57. W. Leemans et al., Phys. Rev. Lett. **113**, 245002 (2014)
58. J.D. Jackson, *Classical Electrodynamics* (Wiley, New York, 1998)
59. L.A. Gizzi et al., IEEE Trans. Plasma Sci. **39**, 2954 (2011)
60. S.H. Glenzer et al., Phys. Plasmas **6**, 2117 (1999)
61. P. Tomassini, A. Giulietti, D. Giulietti, L.A. Gizzi, Appl. Phys. B **80**, 419 (2005)
62. S.K. Ride, E. Esarey, M. Baine, Phys. Rev. E **52**, 5425 (1995)
63. E. Esarey, S.K. Ride, P. Sprangle, Phys. Rev. E **48**, 3003 (1993)
64. A. Macchi, *A Superintense Laser-Plasma Interaction Theory Primer* (Springer, London, 2013)
65. L.D. Landau, E.M. Lifshitz, *The Classical Theory of Fields* (Elsevier, Oxford, 1975)
66. A. Di Piazza, K. Hatsagortsyan, C. Keitel, Phys. Rev. Lett. **102**, 254802 (2009)
67. R.H. Milburn, Phys. Rev. Lett. **10**, 75 (1963)
68. C. Bemporad, R.H. Milburn, N. Tanaka, M. Fotino, Phys. Rev. **138**, B1546 (1965)
69. W.P. Leemans, Phys. Rev. Lett. **67**, 1434 (1991)
70. P. Tomassini et al., Phys. Rev. Spec. Top. Accel. Beams **6**, 121301 (2003)
71. L. Labate et al., Nucl. Instrum. Methods Phys. Res. Sect. A. Accel. Spectrom. Detect. Assoc. Equip. **495**, 148 (2002)
72. S. Chen et al., Phys. Rev. Lett. **155003**, 1 (2013)
73. C. Liu et al., Opt. Lett. **39**, 4132 (2014)
74. N.D. Powers et al., Nat. Photonics **8**, 28 (2013)
75. K. Khrennikov et al., Phys. Rev. Lett. **114**, 1 (2015)
76. D.J. Corvan, G. Sarri, M. Zepf, Rev. Sci. Instrum. **85**, 1 (2014)